# Insights into Size-dependent Activity and Active Sites of Au Nanoparticles Supported on TS-1 for Propene Epoxidation with $H_2$ and $O_2$

Xiang Feng[a], Xuezhi Duan[a], Gang Qian[a], Xinggui Zhou[a,*], De Chen[b], Weikang Yuan[a]

[a] *State Key Laboratory of Chemical Engineering, East China University of Science and Technology, 130 Meilong Road, Shanghai 200237, China*

[b] *Department of Chemical Engineering, Norwegian University of Science and Technology, Trondheim 7491, Norway*

**Abstract**: Propene epoxidation with $H_2/O_2$ is a typical structure-sensitive reaction. For a given support containing tetra-coordinated Ti species such as TS-1, the catalytic activity is greatly influenced by supported Au nanoparticle size. The identification of size-dependent activity of Au catalyst was achieved over a series of Au nanoparticles (2.6-5.1 nm) deposited on the exterior surface of TS-1 by employing uncalcined TS-1. Through this approach, we could obtain very stable Au catalysts with distinguishable and uniform-sized Au particles, which are critical for structure-sensitivity analysis. The PO formation rate ($mol_{PO}s^{-1}mol_{Au}^{-1}$) over these catalysts was found to vary with average Au diameter (d) as $d^{-2.7\pm0.3}$. Moreover, typical Au nanoparticles on uncalcined TS-1 appeared as truncated cuboctahedron with top facet of (111). Model calculations derived from the representative Au particle shape and the above size-dependent activity were then performed to show that corner sites of Au nanopartices are dominant Au active sites for propene expoxidation.

**Keywords**: Propene epoxidation; Uncalcined TS-1; Size-dependent activity; Au active sites; Corner sites

[*]Corresponding author. Tel.: +86-21-64253509. Fax.: +86-21-64253528. E-mail address: xgzhou@ecust.edu.cn

# 1 Introduction

Propene oxide (PO), an important bulk chemical intermediate in petrochemical industries, is widely used to produce polyurethane and polyester resins [1]. In contrast to the traditional chlorohydrin process and several organic hydroperoxide processes for PO production, direct propene epoxidation with molecular $H_2$ and $O_2$ is more attractive because it is environmentally friendly and simple [2]. The catalysts for this reaction require both nano-sized Au particles and tetra-coordinated Ti-containing support [3-16], and the reaction follows a two-site mechanism [1, 17-19]: $H_2$ reacting with $O_2$ to form hydrogen peroxide ($H_2O_2$) at the Au sites, and the $H_2O_2$ subsequently diffusing to the nearby $Ti^{4+}$ sites to generate Ti-OOH species for propene epoxidation. The former step (i.e., the formation of $H_2O_2$) on the Au nanoparticles is the initiation step [1, 17]. The catalytic performance of Au/Ti-containing catalysts for this reaction is typically structure-sensitive to the size and shape of Au nanoparticles [9, 20-22].

To date, considerable efforts have contributed to remarkably improving the catalytic activity by tuning the size of Au nanoparticles deposited on Ti-containing supports [4, 20, 22-25]. This encourages us to further probe the Au size-dependent activity in order to exactly predict the maximum mass specific reactivity. To this end, two major issues for the Au catalysts need to be satisfied: (1) good stability to accurately analyze the catalytic activity and (2) nonporous and highly crystalline support to ensure that all Au nanoparticles could have access to reactants and be observed on the external surface of the support, favoring the precise determination of the Au size distribution by high-resolution transmission electron microscopy (HRTEM) [26, 27]. Fortunately, we have demonstrated that by using uncalcined TS-1 (TS-1-B) as support, the Au nanoparticles are prevented from entering into the micropores [3]. In addition to the

improved size uniformity, the Au nanopartices are on the exterior surface of TS-1 and hence accessible to reactants and easily detected under HRTEM. Moreover, the obtained Au catalyst is stable over 30 h, long enough for a reliable evaluation of the stable catalyst activity. As a consecutive effort, further depositing different sized Au nanoparticles on TS-1-B for the reaction and then obtaining the intrinsic size-dependent activity will be carried out in this work.

Recently, Delgass et al. [28] pointed out that the active sites of Au/TS-1 catalysts for propene epoxidation with $H_2/O_2$ are different from those for CO oxidation. However, the actual active sites (e.g., corner, edge and surface sites) for propene epoxidation are still unknown, and thus the identification of Au active sites is highly desirable for the rational design of highly efficient Au/TS-1 catalysts. It is reported that the supported Au catalysts prepared by deposition-precipitation (DP) method usually exhibit different well-defined Au shapes, which were reported to be affected by the support and preparation parameters [26, 27, 29-31]. To date, it is unclear what the shape of Au nanoparticles deposited on TS-1-B support is. When the Au shape is determined by HRTEM, a physical model could be employed to determine the fraction of different types of sites with the change of Au particle size [32-34]. Furthermore, model calculations derived from the above mentioned size-dependent activity and fraction of different types of sites with particle size could also be performed to investigate the active sites (i.e., corner, edge and surface sites) of Au nanoparticles [26, 27].

In this work, we first employ uncalcined TS-1 with blocked micropores and high crystallinity to support different-sized Au nanoparticles by DP method, and then test the activity of direct propene epoxidation with $H_2$ and $O_2$. The Au/uncalcined TS-1

catalyst has not only uniform and HRTEM visible Au nanoparticles enabling accurate determination of particle size, but also stable catalytic performance enabling reliable determination of Au catalytic activity. In addition, all the Au nanoparticles are exposed on the external surfaces, and thus the observed activity is free from the influence of pore diffusion. Therefore, the intrinsic size-dependent activity of the catalyst is obtained. Subsequently, we use HRTEM to characterize the shape of Au nanoparticles, and thus obtain the fraction of different types of Au sites based on the Au particle shape. Furthermore, combining the size-dependent activity and the fraction of different types of Au sites, we perform calculations to predict the dominant active sites of Au nanoparticles.

## 2 Experimental

### *2.1 Synthesis of TS-1 supports*

TS-1 with a Si/Ti molar ratio of 100 was synthesized according to the previous report [35]. In a typical process, 2.0 g polyoxyethylene 20-sorbitan monolaurate (Tween 20, Aldrich) was first dissolved in 28.6 mL deionized water. To this clear solution, a mixture of 22.6 g tetrapropylammonium hydroxide (TPAOH, 25 wt%) and 173 mmol tetraethylorthosilicate (TEOS, 95 wt%) was added, and then the solution was vigorously stirred at room temperature. After stirring for 0.5 h, 1.73 mmol titanium (IV) tetrabutoxide (TBOT, 99 wt%) dissolved in 20 mL isopropanol (WAKO, 99.5 wt%) was added drop-wise. The solution was crystallized in a Teflon autoclave at 443 K for over 18 h. The as-synthesized TS-1 was thoroughly washed with deionized water and dried overnight at room temperature. It had micropores blocked by the remaining template and hence denoted as TS-1-B. After it was further

subjected to calcination at 823 K for 5.5 h, the template in the TS-1-B was removed. The obtained TS-1 had open micropores and was therefore denoted as TS-1-O.

*2.2 Synthesis of Au/TS-1-B catalysts*

Au/TS-1-B catalysts were prepared by the deposition-precipitation method according to the previous report [24]. 0.1 g $HAuCl_4 \cdot 3H_2O$ was first dissolved in 50 mL deionized water at room temperature, followed by addition of 0.5 g TS-1-B supports. Then, the pH of the slurry was adjusted to 7.3-7.5 by 1 M sodium hydroxide solution. The slurry was further aged for different hours to tune the Au loadings, while the pH of the slurry was kept constant. Finally, the solid was centrifuged for 30 min, washed twice with 50 mL deionized water and dried at room temperature overnight under vacuum. The as-obtained Au/TS-1-B catalysts had different Au loadings of 0.06, 0.12, 0.20, 0.24 and 0.40 wt%.

*2.3 Characterization*

The crystal phases of TS-1-B and TS-1-O supports were characterized by XRD (Rigaku D/Max2550VB/PC, Cu $K_\alpha$ radiation). The surface areas and pore volumes of the supports and Au catalysts were measured in a volumetric adsorption unit (Micromeritics ASAP 2020). The Au loadings were determined by AAS (ZEEnit 600). High-resolution transmission electron microscopy (HRTEM) images were obtained on a JEOL JSM-2010. High-angle annular dark-field scanning transmission electron microscopy (HAADF-STEM) images were obtained on a Tecnai G2 F20 S-Twin equipped with a digitally processed STEM imaging system.

*2.4 Catalytic testing*

Au/TS-1-B catalysts with different average Au particle sizes were tested in a quartz tubular reactor (i.d. 8 mm) loading 0.15 g catalyst of 60-80 mesh particle size. The reactor was heated from room temperature to 200 $^{o}$C at a rate of 0.5 $^{o}$Cmin$^{-1}$. Testing of the catalytic performance for gas-phase propene epoxidation was then conducted at 200 $^{o}$C under atmosphere pressure, with a feed concentration of 10/10/10/70 vol.% of $C_3H_6$, $H_2$, $O_2$ and $N_2$, and at a space velocity of 14,000 $mLh^{-1}g_{cat}^{-1}$. The feed and product concentrations were measured online by two gas chromatographs (Agilent 6890). One chromatograph equipped with thermal conductivity detectors (TCD) was used to detect hydrocarbons, $H_2$, $O_2$, $N_2$, $CO_x$ and $H_2O$ with a 5A column (3 mm × 3 m) and a Porapak Q column (3 mm × 3 m). The other equipped with a flame ionization detector (FID) was used to detect oxygenates (e.g., propene, propane, acetaldehyde, PO, acetone and propanal) with a Porapak T column (3 mm × 3 m).

## 3 Results and discussion

### *3.1 Size-dependent activity of Au/TS-1-B catalyst*

Fig. 1a shows the XRD spectra of the TS-1-B and TS-1-O supports. Similar to traditional crystalline TS-1-O support, the TS-1-B support is also highly crystalline with standard MFI structure. The presence of the orthorhombic symmetry is evidenced by the lack of splitting peaks at ca. 24.5$^{o}$ [35]. Fig. 1b shows the $N_2$ adsorption-desorption isotherms of both TS-1-B and TS-1-O supports. The TS-1-B support is almost nonporous, as indicated by the very small uptake in the isotherm at $P/P_0 < 0.02$ and the negligible micropore volume (i.e., 0.01 $cm^3g^{-1}$) compared with that of traditional TS-1-O support (i.e., 0.23 $cm^3g^{-1}$). As explained in Ref. [36], the

nonporous characteristic of the TS-1-B support is because the micropores are blocked by TPA template, with its nitrogen atom at the center of channel intersection and the propyl groups extending along the channels.

(Fig. 1 should be inserted here)

The highly crystalline structure of the TS-1-B support provides a sharp contrast between Au nanoparticles and support. Moreover, the blocked micropores guarantee that all nanoparticles are on the exterior surface and thus no tiny Au nanoparticles could be hidden from view inside the micropores [26]. Therefore, counting the Au nanoparticles observed under HRTEM will give a reliable particle size. Fig. 2(a-e) presents the typical HRTEM images of Au/TS-1-B catalysts with different Au loadings. For each catalyst, the entire Au nanoparticles observed by HRTEM were counted for averaged particle size to reduce statistical error. The average Au particle size are ranged from 2.6 to 5.1 nm with increasing Au loading from 0.06 to 0.40 wt%.

(Fig. 2 should be inserted here)

Because of the high detection limit of the HRTEM [23], the Au nanoparticles smaller than 0.8 nm which are also active towards PO production are difficult to be identified and counted. To estimate the statistical error, we have used high-angle annular dark-field (HAADF) scanning transmission electron microscopy (STEM) with resolution of 0.20 nm to determine the fraction of the tiny Au particles. Fig. 2f and Fig. S1 show the images of the Au/TS-1-B catalyst with Au loading of 0.06%. When we count over 200 Au particles from HAADF-STEM images, we find that only less than 1% Au nanoparticles are smaller than 0.8 nm. This is in accordance with the work of Ribeiro et al. that Au catalysts prepared by deposition-precipitation (DP)

method lack subnanometer Au particles [26]. The calculated average Au sizes by HAADF-STEM and HRTEM images are almost the same. Therefore, the averaged Au sizes mentioned below are based on the observation by HRTEM.

Fig. 3 shows the activities ($mol_{PO}s^{-1}mol_{Au}^{-1}$) of the five Au/TS-1-B catalysts for a period of 14 hours, which are presented as the PO formation rate per mole of Au. These catalysts are very stable mainly because Au nanoparticles are on the external surface of the support, which avoids the deactivation caused by micropore blocking [3]. When these catalysts were prepared, only the Au loadings were varied, and other preparation and evaluation conditions were kept the same. Therefore, the difference in the activities are due to the different loadings, and furthermore the sizes of the Au nanoparticles. Fig. 4a shows the PO selectivity and $H_2$ efficiency of Au/TS-1-B catalysts varying with Au particle size. The PO selectivity decreases remarkably from 89.6 to 65.0 % when the Au particle size increases from 2.6 to 5.1 nm, and the $H_2$ efficiency decreases from 33.6 to 13.0 %. The obvious trend of the PO formation rate ($mol_{PO}s^{-1}mol_{Au}^{-1}$) decreasing with the average Au particle size (d) as $d^{-2.7\pm0.3}$ at 200 $^{o}$C is shown in Fig. 4b. It should be noted that the minimum average Au particle size in this work is ca. 2.6 nm. Extrapolating the activity for a smaller Au nanoparticle size of 2.49 nm gives a value of 0.17 $mol_{PO}s^{-1}mol_{Au}^{-1}$, quite close to the reported ca. 0.15 $mol_{PO}s^{-1}mol_{Au}^{-1}$ for 0.031 wt% Au/TS-1 catalyst by Delgass et al. [24], indicating the accuracy of the size-dependent activity. The little difference may be attributed to the inaccurate size determination or the fast catalyst deactivation which continuously changes the activity of Au/TS-1 catalyst.

(Fig. 3 should be inserted here)

(Fig. 4 should be inserted here)

*3.2 Active sites on Au nanoparticles*

The catalytic activity of Au/TS-1-B catalysts has been shown to be size-dependent. Understanding the origin of the size-dependent activity will undoubtedly help to optimize the performance of the catalyst. Very possibly, the size effect may originate from the size-dependent number of distinct sites (e.g., corner, edge, perimeter and surface sites) on a gold particle [26, 27] since the rate-relevant step (i.e., $H_2O_2$ synthesis by $H_2$ and $O_2$) is on Au nanoparticles (Fig. S3). For an easy start, we check whether these sites can account for the size-dependent activity.

Here we introduce turnover rate (TOR) for discussion, which is the molar PO formation rate per mole of Au surface sites. It can be calculated by dividing the PO formation rate on the basis of per mole Au atoms ($mol_{PO}s^{-1}mol_{Au}^{-1}$) by the Au dispersion, (i.e., the moles of active site per mole of Au surface atoms). As is well known that the Au dispersion is difficult to be determined by chemisorption because the chemisorption of many molecules such as $H_2$ and CO on Au nanoparticles is non-quantitative [37, 38]. Instead, the dispersion for Au catalysts with regular shape is assumed to vary reciprocally with d [26, 39], as is widely accepted in the Au catalysis community. Therefore, the TOR can be readily obtained by multiplying the PO formation rate by d. If corner, edge, perimeter and surface sites have the same activity, the TOR should be independent of particles size, and the PO formation rate per mole Au atoms should vary as $d^{-1}$. However, the PO formation rate changes with d as $d^{-2.7\pm0.3}$ (Fig. 4b), indicating that these sites are not uniformly active. Indeed, the corner, edge, perimeter and surface sites have different coordination numbers and usually exhibit different activities. One can assume that only one of the four types of sites contributes mostly to the overall activity of the catalyst.

To determine which type of site is responsible for the size-dependent activity, it is necessary to determine quantitatively how the fraction of a specific site type changes with particle size. Nevertheless, fraction can only be determined when the particle shape is known. Fig. 5 and Fig. S2 shows the representative Au shape observed by HRTEM, which is best represented by the top slice of truncated cuboctahedron. This is usually observed for Au catalysts prepared by DP method because it has minimum surface free energy for fcc metals [40]. From the FFT of the selected area and HRTEM observations (Fig. 5) and the representative Au truncated cuboctahedron shapes (Fig. 6), the Au particle of Au/TS-1-B catalyst shows top facet of (111). It is possible to calculate the fraction of atoms in a particular configuration (i.e., corner, edge or surface sites) from a simple Au physical model [32-34]. The model are based on three principles: (1) Even in the smallest crystallites the metal atoms occupy crystallographic positions; (2) The particles are constructed of a fixed, predetermined number of atoms; (3) The crystallites are so shaped that their free energy is a minimum. The fractions of different types of sites from the physical model are shown in Table S1 and Fig. S3.

(Fig. 5 should be inserted here)

(Fig. 6 should be inserted here)

By assuming that only one type of site accounts for the activity of Au catalysts and the PO formation rate of one specific type of active site (e.g., corner site) is uniform regardless of Au particle size [27, 41], the PO formation rate will then change only with the fraction of Au specific sites. In other words, with the known correlation between the fraction of Au specific sites and the average Au diameter, it is possible for us to further predict the relation between PO formation rate and average Au

diameter.

Denoting $C_{site}$ as the PO formation rate of a specific active site, and *s(d)* and *t(d)* as the number of the specific sites and the number of total atoms on an Au nanoparticle with diameter of d, respectively, the PO formation rate of a catalyst (i.e., $r_{PO}$ on the basis of per molar Au) can be described as follows:

$$r_{PO} = C_{site} \cdot \left[\sum s(d)\right] / \left[\sum t(d)\right]$$

We could fit the experiments with the site models to minimize the squared residual between the experiments and the site models:

$$\min_{C_{site}} \left\{ r_{PO}(\exp) - C_{site} \left[\sum s(d) / \sum t(d)\right] \right\}^2$$

The constant $C_{site}$ can be calculated from the best fit of the site model to the experimentally determined PO formation rate of Au/TS-1-B catalysts. The calculated PO formation rate on different types of site models as a function of average Au diameter was shown in Fig. 7. The PO formation rate on corner sites varies with d as $d^{-3}$, which correlates very well with the experimental result (i.e., $d^{-2.7}$). Moreover, because the surface site, edge site and perimeter site models all give a weaker size dependence than experiments, any multiple-site model involving any two, three or four sites will be inferior to the corner site model in fitting the experiments. Therefore, it is suggested that among all the four sites, the corner sites are dominant Au active sites for PO formation. It should be noted that the Au corner sites that are most close to support may favor the transmission of $H_2O_2$ to nearby $Ti^{4+}$ sites.

(Fig. 7 should be inserted here)

For these low-coordinate Au corner sites, oxygen is more easily adsorbed, as reported by Nørskov et al. [34]. As a result, the rate-relevant step of propene epoxidation (i.e., $H_2O_2$ production by oxygen and hydrogen on Au particles) could be facilitated. This could further confirm that the Au corner sites are the dominant active sites. Moreover, it is known that the number of corner sites on one Au nanoparticle is independent of the Au particle size. This means that the higher PO formation rate per mole Au atoms with smaller Au particle size is primarily due to the growth of corner sites number. Notably, the decrease of particle size in the range of 2.6 and 5.1 nm does not induce the quantum-size effect, which ascribes the particle-size dependent TOF to the change of electronic structure. This is because the quantum-size effect is often crucial for tiny particles with small number of atoms (e.g., 6 atoms) [34, 42]. Therefore, it is feasible to explain the size dependence on catalytic activity without the necessity to involve the change of electronic nature for the Au nanoparticles in this work. In addition, it can be seen from Fig. 4a that the non-selective oxidation is facilitated and the $H_2$ efficiency is reduced on larger Au particles. This may be because some of hydrogen peroxide formed on larger Au nanoparticles goes a longer way by surface diffusion to the nearby $Ti^{4+}$ sites for propene epoxidation. Therefore, on larger nanoparticles the possibility of non-selective oxidation of propene to side products or decomposition to $H_2O$ is increased owing to the longer pathway of surface diffusion [9]. These results offer a new direction of designing more effective Au catalysts for propene epoxidation by preparing small Au nanoparticles that process higher fraction of low-coordinate corner sites.

## 4 Conclusions

In summary, the size-dependent PO formation rate per mole of Au atoms

($mol_{PO}s^{-1}mol_{Au}^{-1}$) for propene epoxidation with $H_2$ and $O_2$ was found to vary with Au diameter (d) as $d^{-2.7\pm0.3}$ in the range of 2.6 and 5.1 nm. This was achieved by depositing Au nanoparticles on the external surface of uncalcined TS-1 with blocked micropores which has good catalytic stability and nonporous support with high crystallinity for structure-sensitivity analysis. In addition, the truncated cuboctahedron shape with top facet of (111) is found to be the dominate Au shape by HRTEM. Based on the Au shape and Au size-dependent activity, calculations were performed and showed that Au corner sites are the dominant Au active sites. The higher PO formation rate per mole Au atoms with smaller Au particle size is primarily due to the high fraction of corner sites number.

## Acknowledgments

This work is financially supported by the 973 Program (2012CB720501), the Natural Science Foundation of China (U1162112) and the 111 Project of Ministry of Education of China (B08021).

## References

[1] T.A. Nijhuis, M. Makkee, J.A. Moulijn, B.M. Weckhuysen, Ind. Eng. Chem. Res. 45 (2006) 3447-3459.
[2] B. Chowdhury, K. Bando, J. Bravo-Suárez, S. Tsubota, M. Haruta, J. Mol. Catal. A: Chem. 359 (2012) 21-27.
[3] X. Feng, X. Duan, G. Qian, X. Zhou, D. Chen, W. Yuan, Appl. Catal., B 150 (2014) 396-401.
[4] W.-S. Lee, L.-C. Lai, M. Cem Akatay, E.A. Stach, F.H. Ribeiro, W.N. Delgass, J. Catal. 296 (2012) 31-42.
[5] G. Zhan, M. Du, D. Sun, J. Huang, X. Yang, Y. Ma, A.-R. Ibrahim, Q. Li, Ind. Eng. Chem. Res. 50 (2011) 9019-9026.
[6] L. Xu, Y. Ren, H. Wu, Y. Liu, Z. Wang, Y. Zhang, J. Xu, H. Peng, P. Wu, J. Mater. Chem. 21 (2011) 10852-10858.
[7] H. Yang, D. Tang, X. Lu, Y. Yuan, J. Phys. Chem. C 113 (2009) 8186-8193.
[8] E. Sacaliuc, A.M. Beale, B.M. Weckhuysen, T.A. Nijhuis, J. Catal. 248 (2007) 235-248.
[9] J. Lu, X. Zhang, J.J. Bravo-Suárez, K.K. Bando, T. Fujitani, S.T. Oyama, J. Catal. 250 (2007) 350-359.

[10] G. Qian, Y.H. Yuan, W. Wu, X.G. Zhou, Stud. Surf. Sci. Catal. 159 (2006) 333-336.
[11] Y.-H. Yuan, X.-G. Zhou, W. Wu, Y.-R. Zhang, W.-K. Yuan, L. Luo, Catal. Today 105 (2005) 544-550.
[12] B.S. Uphade, T. Akita, T. Nakamura, M. Haruta, J. Catal. 209 (2002) 331-340.
[13] G. Mul, A. Zwijnenburg, B. van der Linden, M. Makkee, J.A. Moulijn, J. Catal. 201 (2001) 128-137.
[14] T.A. Nijhuis, B.J. Huizinga, M. Makkee, J.A. Moulijn, Ind. Eng. Chem. Res. 38 (1999) 884-891.
[15] A.K. Sinha, S. Seelan, S. Tsubota, M. Haruta, Angew. Chem., Int. Ed. 43 (2004) 1546-1548.
[16] W.-S. Lee, M. Cem Akatay, E.A. Stach, F.H. Ribeiro and W. Nicholas Delgass, J. Catal. 313 (2014) 104-112.
[17] J.J. Bravo-Suarez, K.K. Bando, J. Lu, M. Haruta, T. Fujitani, T. Oyama, J. Phys. Chem. C 112 (2008) 1115-1123.
[18] A. Ruiz, B. van der Linden, M. Makkee, G. Mul, J. Catal. 266 (2009) 286-290.
[19] J. Chen, S.J. Halin, E.A. Pidko, M. Verhoeven, D.M.P. Ferrandez, E.J. Hensen, J.C. Schouten and T.A. Nijhuis, ChemCatChem, 5 (2013) 467-478.
[20] X. Lu, G.-F. Zhao and Y. Lu, Catal. Sci. Technol. 3 (2013) 2906-2909.
[21] C. Qi, T. Akita, M. Okumura, K. Kuraoka, M. Haruta, Appl. Catal., A 253 (2003) 75-89.
[22] J. Huang, E. Lima, T. Akita, A. Guzmán, C. Qi, T. Takei, M. Haruta, J. Catal. 278 (2011) 8-15.
[23] J. Huang, T. Takei, T. Akita, H. Ohashi, M. Haruta, Appl. Catal., B 95 (2010) 430-438.
[24] W.-S. Lee, M. Cem Akatay, E.A. Stach, F.H. Ribeiro, W. Nicholas Delgass, J. Catal. 287 (2012) 178-189.
[25] W.-S. Lee, M. Cem Akatay, E.A. Stach, F.H. Ribeiro, W. Nicholas Delgass, J. Catal. 308 (2013) 98-113.
[26] M. Shekhar, J. Wang, W.-S. Lee, W.D. Williams, S.M. Kim, E.A. Stach, J.T. Miller, W.N. Delgass, F.H. Ribeiro, J. Am. Chem. Soc. 134 (2012) 4700-4708.
[27] W.D. Williams, M. Shekhar, W.-S. Lee, V. Kispersky, W.N. Delgass, F.H. Ribeiro, S.M. Kim, E.A. Stach, J.T. Miller, L.F. Allard, J. Am. Chem. Soc. 132 (2010) 14018-14020.
[28] W.-S. Lee, R. Zhang, M.C. Akatay, C.D. Baertsch, E.A. Stach, F.H. Ribeiro, W.N. Delgass, ACS Catal. 1 (2011) 1327-1330.
[29] R. Zanella, S. Giorgio, C.-H. Shin, C.R. Henry, C. Louis, J. Catal. 222 (2004) 357-367.
[30] W. Deng, A.I. Frenkel, R. Si, M. Flytzani-Stephanopoulos, J. Phys. Chem. C 112 (2008) 12834-12840.
[31] N. Patil, B. Uphade, D. McCulloh, S. Bhargava, V. Choudhary, Catal. Comm. 5 (2004) 681-685.
[32] R. Van Hardeveld, F. Hartog, Surf. Sci. 15 (1969) 189-230.
[33] A. Carlsson, A. Puig-Molina, T.V. Janssens, J. Phys. Chem. B 110 (2006) 5286-5293.
[34] T.V. Janssens, B.S. Clausen, B. Hvolbæk, H. Falsig, C.H. Christensen, T. Bligaard, J.K. Nørskov, Top.Catal. 44 (2007) 15-26.
[35] R.B. Khomane, B.D. Kulkarni, A. Paraskar, S.R. Sainkar, Mater. Chem. Phys. 76 (2002) 99-103.
[36] L. Parker, D. Bibby, J. Patterson, Zeolites 4 (1984) 168-174.
[37] T. Choudhary, D. Goodman, Appl. Catal., A 291 (2005) 32-36.
[38] F. Menegazzo, M. Manzoli, A. Chiorino, F. Boccuzzi, T. Tabakova, M. Signoretto, F. Pinna, N. Pernicone, J. Catal. 237 (2006) 431-434.
[39] S. Overbury, V. Schwartz, D.R. Mullins, W. Yan, S. Dai, J. Catal. 241 (2006) 56-65.
[40] W. Romanowski, Surf. Sci. 18 (1969) 373-388.

[41] N. Lopez, T. Janssens, B. Clausen, Y. Xu, M. Mavrikakis, T. Bligaard, J.K. Nørskov, J. Catal. 223 (2004) 232-235.
[42] X. Wu, L. Senapati, S. Nayak, A. Selloni, M. Hajaligol, J. Chem. Phys. 117 (2002) 4010-4015.

**Figure captions:**

**Fig. 1.** (a) XRD patterns and (b) $N_2$ adsorption-desorption isotherms of TS-1-B and TS-1-O supports. The insets in Fig. 1b show the schemes of the framework structure of the two supports.

**Fig. 2.** Representative HRTEM images of the used Au/TS-1-B catalysts with Au loadings of (a) 0.06, (b) 0.12 (c) 0.20, (d) 0.24 and (e) 0.40 wt% at 200 $^{o}$C for 4 h. The insets show the particle size distributions of the Au catalysts. (f) HAADF-STEM image for 0.06 wt% Au/TS-1-B catalyst. The HAADF-STEM observation of Au catalyst was carried out after testing at 200 $^{o}$C for 4 h.

**Fig. 3.** Stabilities of Au/TS-1-B catalysts with Au loadings of (a) 0.06, (b) 0.12, (c) 0.20, (d) 0.24 and (e) 0.40 wt% at 200 $^{o}$C.

**Fig. 4.** (a) PO and $H_2$ selectivity and (b) PO formation rate of Au/TS-1-B catalysts with different Au particle sizes.

**Fig. 5.** Typical shape of Au nanoparticles. The insets show FFT of the selected area and the possible Au shape.

**Fig. 6.** Representative truncated cuboctahedron shapes with top facets of (111) (a) and (100) (b). The insets show the facets and the angle between different facets.

**Fig. 7.** PO formation rate of Au/TS-1-B catalysts from calculations and experimental data. The fitting curves are calculated results based on different sites.

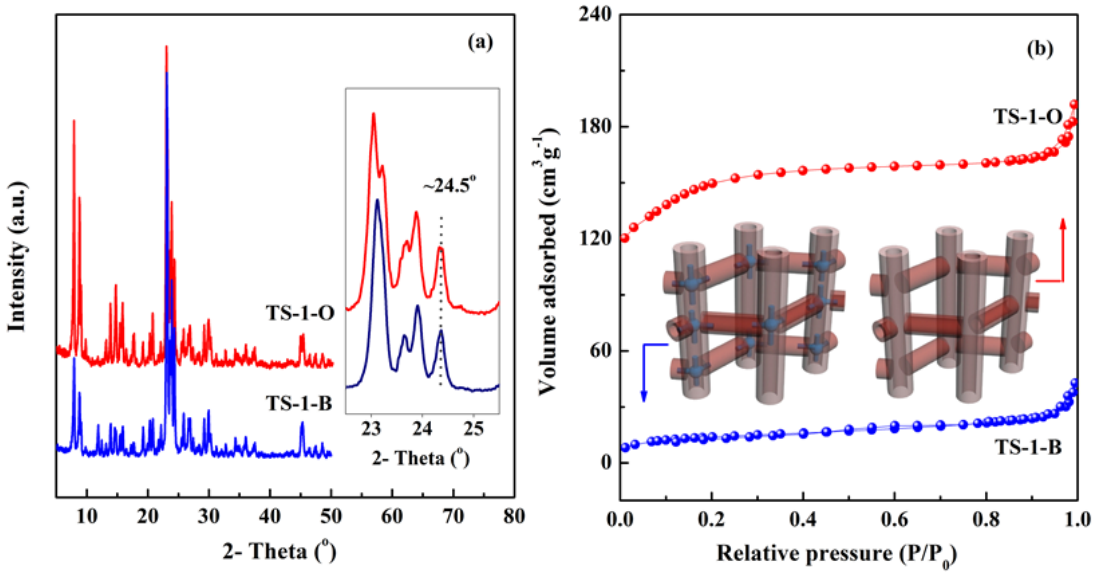


**Fig. 1.** (a) XRD patterns and (b) $N_2$ adsorption-desorption isotherms of TS-1-B and TS-1-O supports. The insets in Fig. 1b show the schemes of the framework structure of the two supports.

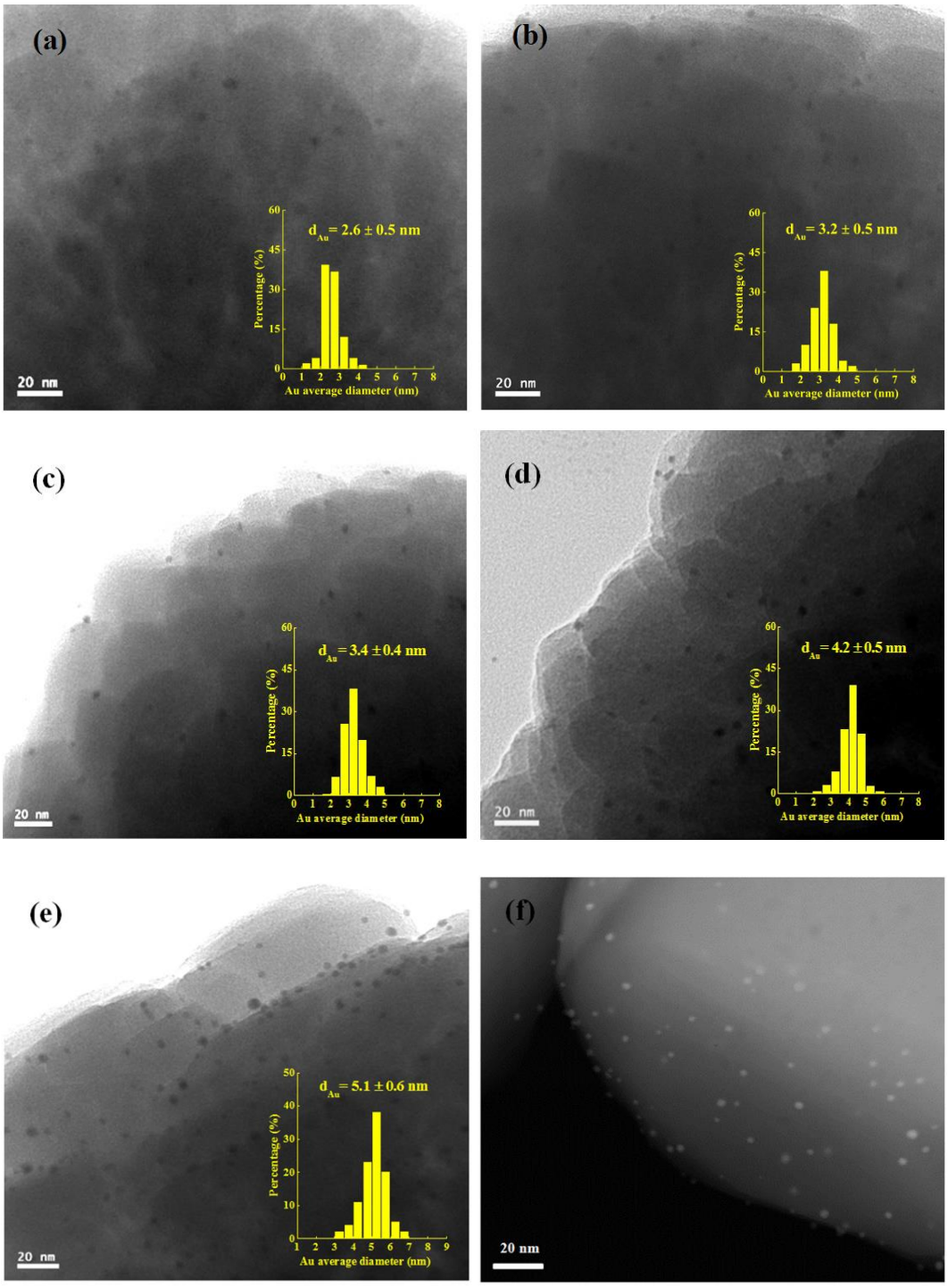


**Fig. 2.** Representative HRTEM images of the used Au/TS-1-B catalysts with Au loadings of (a) 0.06, (b) 0.12 (c) 0.20, (d) 0.24 and (e) 0.40 wt% at 200 ºC for 4 h. The insets show the particle size distributions of the Au catalysts. (f) HAADF-STEM image for 0.06 wt% Au/TS-1-B catalyst. The HAADF-STEM observation of Au catalyst was carried out after testing at 200 ºC for 4 h.

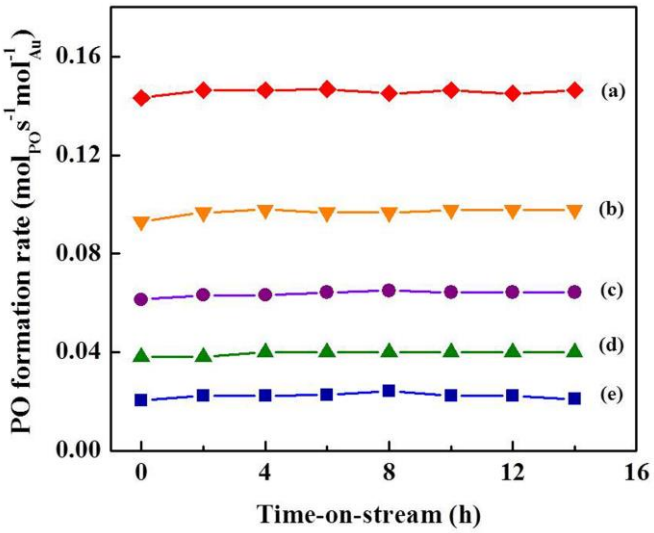


**Fig. 3.** Stabilities of Au/TS-1-B catalysts with Au loadings of (a) 0.06, (b) 0.12, (c) 0.20, (d) 0.24 and (e) 0.40 wt% at 200 $^{o}$C.

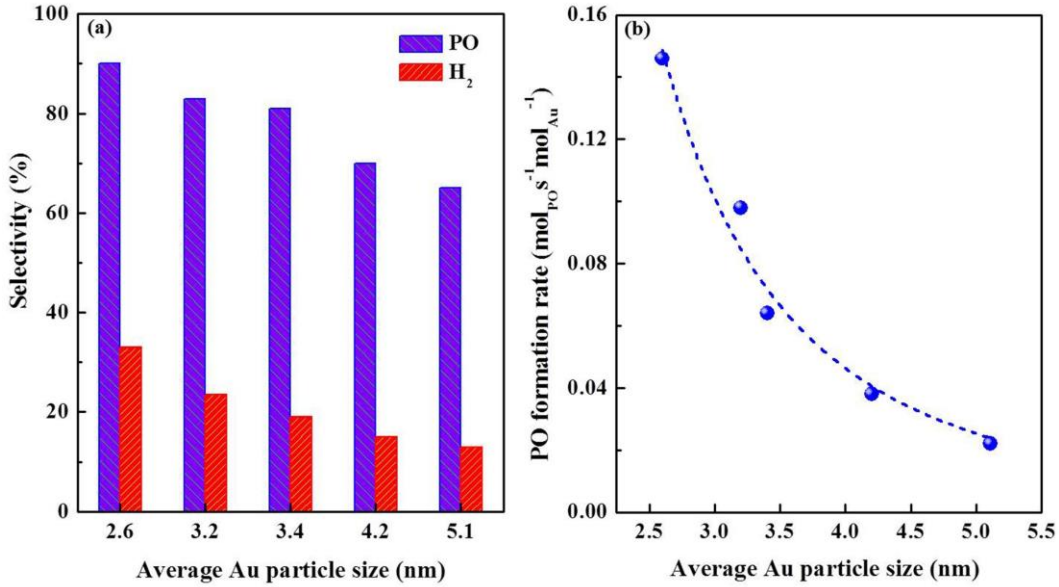


**Fig. 4.** (a) PO and $H_2$ selectivity and (b) PO formation rate of Au/TS-1-B catalysts with different Au particle sizes.

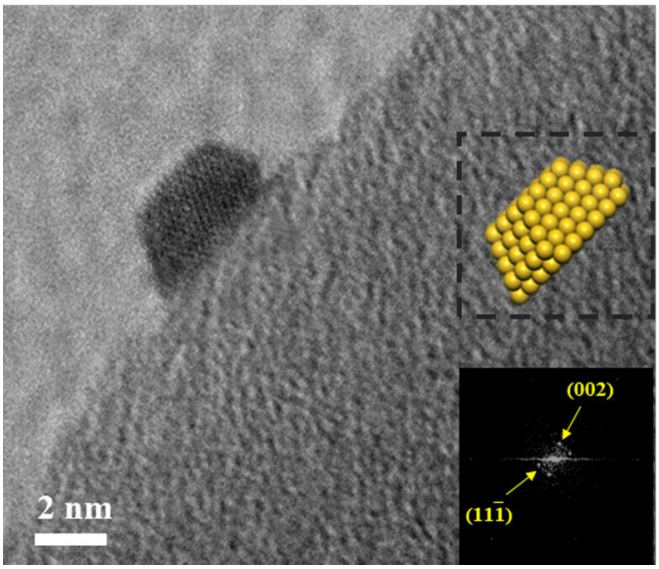


**Fig. 5.** The typical shape of Au nanoparticles. The insets show FFT of the selected area and the possible Au shape.

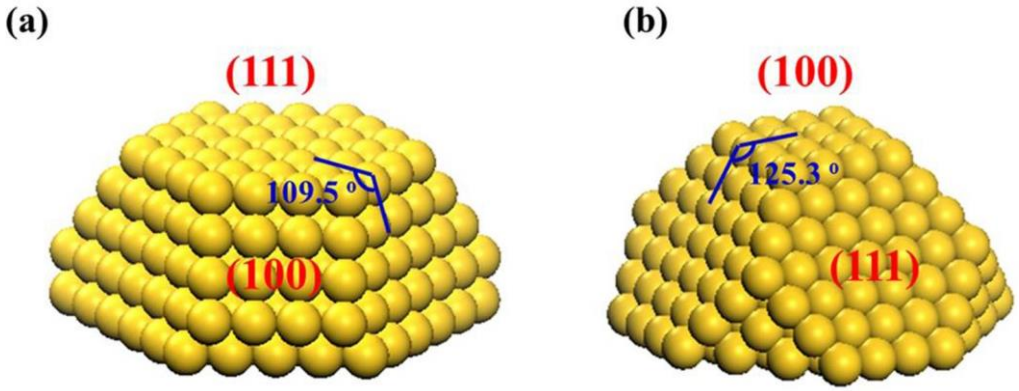


**Fig. 6.** Representative truncated cuboctahedron shapes with top facets of (111) (a) and (100) (b). The insets show the facets and the angle between different facets.

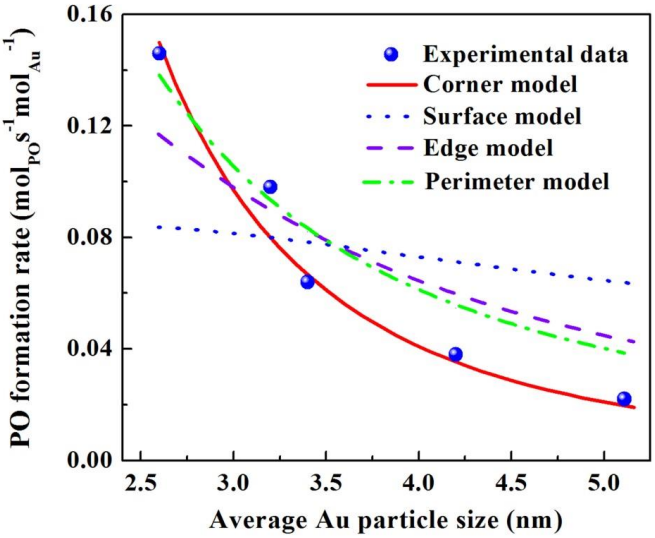


**Fig. 7.** PO formation rate of Au/TS-1-B catalysts from calculations and experimental data. The fitting curves are calculations results based on different sites.